

INVESTIGATION OF THE PHOTOELECTROCHEMICAL BEHAVIOR OF NANOCARBON/MESOPOROUS TiO₂ FILMS

M. SIMA^{*a}, E. VASILE^b, A. SIMA^c

^aNational Institute of Materials Physics, 405A Atomistilor Street, 077125 Magurele, Romania

^bUniversity "Politehnica" of Bucharest, Faculty of Applied Chemistry and Material Science, Department of Oxide Materials and Nanomaterials, No. 1-7 Gh. Polizu Street, 011061 Bucharest, Romania

^cNational Institute for Lasers, Plasma and Radiation Physics, 409 Atomistilor Street, P.O. Box MG-36 077125 Magurele, Romania

In this work, we report the influence of nanocarbon deposited on mesoporous TiO₂ by spray method on photoelectrochemical performance of the formed photoanodes. Scanning electron microscopy and transmission electron microscopy images confirmed presence of carbon nanoparticles on the surface of anatase TiO₂ films. Nanocarbon decorated TiO₂ photoanodes were characterized by electrochemical impedance spectroscopy and Mott-Schottky analysis. Charge recombination process was evaluated by measurement of open-circuit voltage decay after interruption the illumination. Only a small enhancement of photoelectrochemical performance of these photoanodes was observed. It was attributed to increasing of charge carrier density as a result of nanocarbon deposition on TiO₂ film.

(Received June 14, 2019; Accepted October 23, 2019)

Keywords: Water splitting, Mesoporous TiO₂, Nanocarbon, Photoanode

1. Introduction

TiO₂ is a natural n-type semiconductor which was widely studied as the key photoanodes for production of solar fuel using photoelectrochemical cells. It has a high chemical and optical stability, low cost and is non-aggressive in the environment and corrosion resistant. The absorption edge of TiO₂ is 3.2 eV [1-3] resulting that only 4% of the incident solar energy can be absorbed by this semiconductor. The positions of the conduction band ($E_{CB}=-0.2V$ vs. reversible hydrogen electrode (RHE)) and valence band ($E_{VB}=3.0 V$ vs. RHE) energies of TiO₂ are suitable for hydrogen generation using only a single photocatalyst in water splitting process [4]. However, water splitting is thermodynamically possible without external bias on TiO₂ anatase only [5]. The electron mobility of TiO₂ film is low, about 0.01 cm²/Vsec [6]. To increase electron mobility [7] it is necessary crystallization of TiO₂ into anatase phase. As a result, two major limitations of TiO₂ semiconductor affect the conversion of photon to hydrogen in water splitting process, namely the wide bandgap and fast recombination of the charge carriers. Several methods have been proposed to improve the photoelectrochemical performance of TiO₂ under visible light irradiation which include [8] semiconductor coupling to TiO₂ [9], ternary TiO₂ photocatalysts [10], metal modified TiO₂ [11] and non-metal modified TiO₂ [12]. The enhanced photoelectrochemical (PEC) performance of semiconductor materials decorated with carbon quantum dots [13-15] was attributed to enlarged absorption range to near infrared region and to increased electrical conductivity of these materials. Also, carbon quantum dots/TiO₂ composite prepared by

* Corresponding author: msima@infim.ro

hydrothermal method showed enhanced catalytic activities in oxidation of alcohols [16]. Carbon contents higher than 4 wt.% have been reported in literature as optimal for degradation of several organic pollutants with carbon-TiO₂ composites [17].

Here, we show the results of PEC characterization of carbon nanoparticles/mesoporous TiO₂ films fabricated via spray coating method and used as photoanodes for water splitting process. Comparatively, nanocarbon/TiO₂ composites with low carbon content were studied.

2. Experimental

2.1. Preparation of photoanodes

Mesoporous TiO₂ layers were deposited on FTO substrate using commercial paste Dyesol 18NR-T diluted further with ethanol absolute (1/6 by weight) [18]. The layers prepared by spin coating technique at 2000 rpm for 60s were annealed in air at 550⁰ C for 1h followed by cooling to room temperature. The carbon quantum dots were prepared in a two-step process comprising the combustion of a flammable solvent and the dispersion of obtained soot in organic solvent. Ethanol was used both as a flammable organic solvent and as dispersing medium for the obtained soot. It was placed in a crucible and burnt in air and the soot was collected into a Berzelius beaker at 10 cm above the crucible [19]. 2 mg of soot were dispersed in 50 ml ethanol and the mixture was stirred 30 min and sonicated 2 h. Then, the dispersion was centrifuged for 3 minutes at 5000 rpm. The undispersed soot was removed and the supernatant was collected. The dispersion of nanocarbon in methanol was sprayed on the substrates heated at 50⁰C. The spraying gun was a stainless steel Iwata HP-SB Plus with 0.2 mm nozzle. Spraying distance was 8 cm and the spraying pressure 5 psi. After spraying deposition, TiO₂/nanocarbon films were treated at 300⁰ C for 30 min.

In another experiment, two different carbon-ethanol dispersions having 1.7 and 3.4 mg nanocarbon/cm³, respectively were used to obtain composites nanocarbon/TiO₂. The ratio Dyesol 18NR-T paste/carbon-ethanol dispersion was 1/6 by weight. The composites films were prepared by spin coating technique at 2000 rpm for 60s and annealing in air at 550⁰ C for 1h followed by cooling to room temperature.

2.2. Structural characterizations

Scanning electron microscopy (SEM) and transmission electron microscopy (TEM) were performed to determine surface morphology using Quanta Inspect scanning electron microscope and Tecnai F30 transmission electron microscope from FEY. X-ray diffraction (XRD) patterns were measured on a Bruker D8 Advance type X-ray diffractometer, in focusing geometry, equipped with copper target X-ray tube and LynxEye one-dimensional detector.

The codes of the prepared and characterized samples are listed in the Table 1.

Table 1. Sample code of the films of TiO₂-nanocarbon supported on FTO.

Sample code	Structure description	Deposition time of nanocarbon films (s)
p1	FTO/TiO ₂	
p1C	Sample p1 with TiO ₂ film decorated with nanocarbon	6
p2	FTO/TiO ₂	
p2C	Sample p2 with TiO ₂ film decorated with nanocarbon	12
p3	FTO/TiO ₂	
p3C	Sample p3 with TiO ₂ film decorated with nanocarbon	24
p4	FTO/TiO ₂ - nanocarbon composite obtained from Dyesol paste with 1% nanocarbon	
p5	FTO/TiO ₂ - nanocarbon composite obtained from Dyesol paste with 2% nanocarbon	

2.3. Photoelectrochemical measurements

In order to measure the photoelectrochemical activity of nanocarbon/TiO₂ films, a three-electrode electrochemical system was used which includes together with working electrode, a reference electrode Ag/AgCl/saturated KCl and a Pt foil as the counter electrode. The aqueous solution of the cell contains 0.5 M Na₂SO₄. The measured potentials were applied to the Ag/AgCl but are reported in this paper against the reversible hydrogen electrode (RHE): $E_{\text{RHE}} = E_{\text{Ag/AgCl}} + 0.059\text{pH} + E_{\text{Ag/AgCl}}^0$, with $E_{\text{Ag/AgCl}}^0 = 0.1976$ V at 25°C and pH 7. The illuminated and immersed area of the photoanodes was 1 cm². The samples were illuminated at the photoanode/electrolyte interface using AM1.5 solar simulator (L.O.T.-Oriel GmbH & Co.KG, Model LS0306 with a 300 W Xe-Arc lamp and an AM1.5-Global filter (LSZ189) with the specification: 1 sun at 18 cm working distance). Linear sweep voltammetry was performed with a voltage scan rate of 20 mVs⁻¹ to obtain the photocurrent-voltage (J-V) curves in the dark and under illumination conditions. A potentiostat/galvanostat Autolab PGSTAT 30 (Eco Chemie) was used to perform these measurements. The electrochemical impedance spectroscopy (EIS) was evaluated under illumination in a frequency range of 100 kHz to 2.4 Hz with amplitude of 10 mV. The obtained data were fitted by an equivalent circuit using the Zview software. Mott-Schottky data were collected at 5 kHz, in the dark.

3. Results and discussion

These studies were conducted on samples (Table 1) having small amounts of carbon that allowed the light to reach the FTO/TiO₂ substrate.

XRD pattern of TiO₂ film (Fig.1a) shows only a diffraction peak located at $2\theta = 25.4$ assigned to (101) crystallographic plane of the tetragonal anatase phase. SEM image from Fig.1b shows morphology of mesoporous TiO₂ layer deposited on FTO substrate and TEM image from Fig 1c shows size and morphology of carbon nanoparticles. In Fig.1d are observed carbon nanoparticles with sizes around 25 nm deposited on TiO₂ layer.

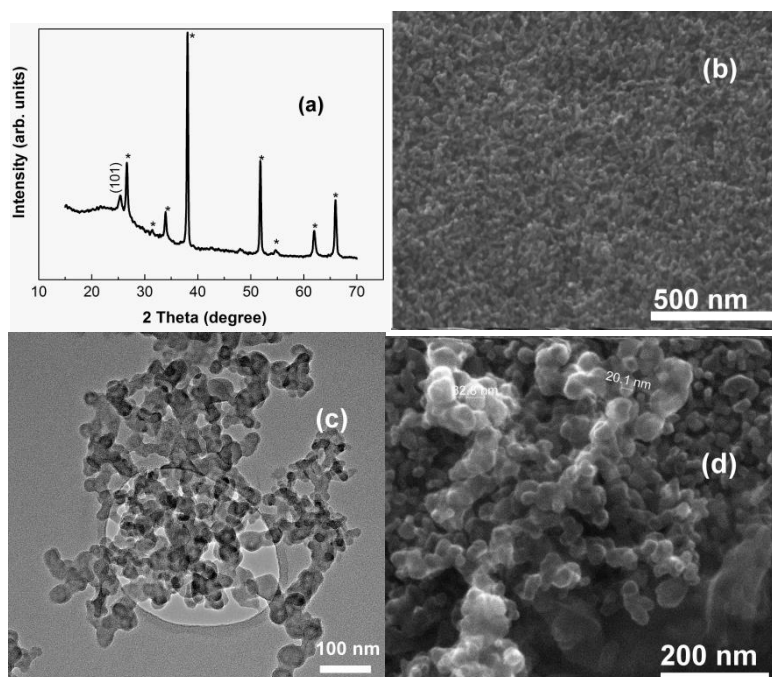


Fig. 1. XRD pattern (a) and SEM image (b) of TiO₂ film on FTO substrate; TEM image of nanoparticles of carbon (c); SEM image of nanoparticles of carbon deposited on TiO₂ film (sample p3C)(d).

Large surface area of mesoporous TiO₂ layer favors both light absorption and charge transfer process at electrode/electrolyte interface. Because TiO₂ samples prepared under the same

conditions (p1, p2, p3) have surfaces with slightly different characteristics, this study compared the samples with the same TiO₂ substrate (p1 with p1C, p2 with p2C, p3 with p3C).

The PEC performance of these photoanodes is shown in Fig.2 a, b, c. Under illumination, the current densities at potential of 1.23V/RHE are close in each pair of photoanodes. There was a slight increase of the photocurrent at 1.23V/RHE only in the case of the p2C sample (0.3 mA/cm²) compared to the sample p2 (0.28 mA/cm²).

We further investigated the PEC properties of the photoanodes using electrochemical impedance measurements. Figs.2 d, e, f show the Nyquist representations of the impedance spectra of the photoanodes under simulated solar illumination conditions, in 0.5 M Na₂SO₄ solution, at a potential of 1.23 V vs RHE. These impedance spectra mainly reveal a charge transfer phenomenon: charge transfer at electrode/electrolyte interface (arc at lower frequencies). The equivalent circuit used to fit the impedance data is showed in the Fig. 2d.

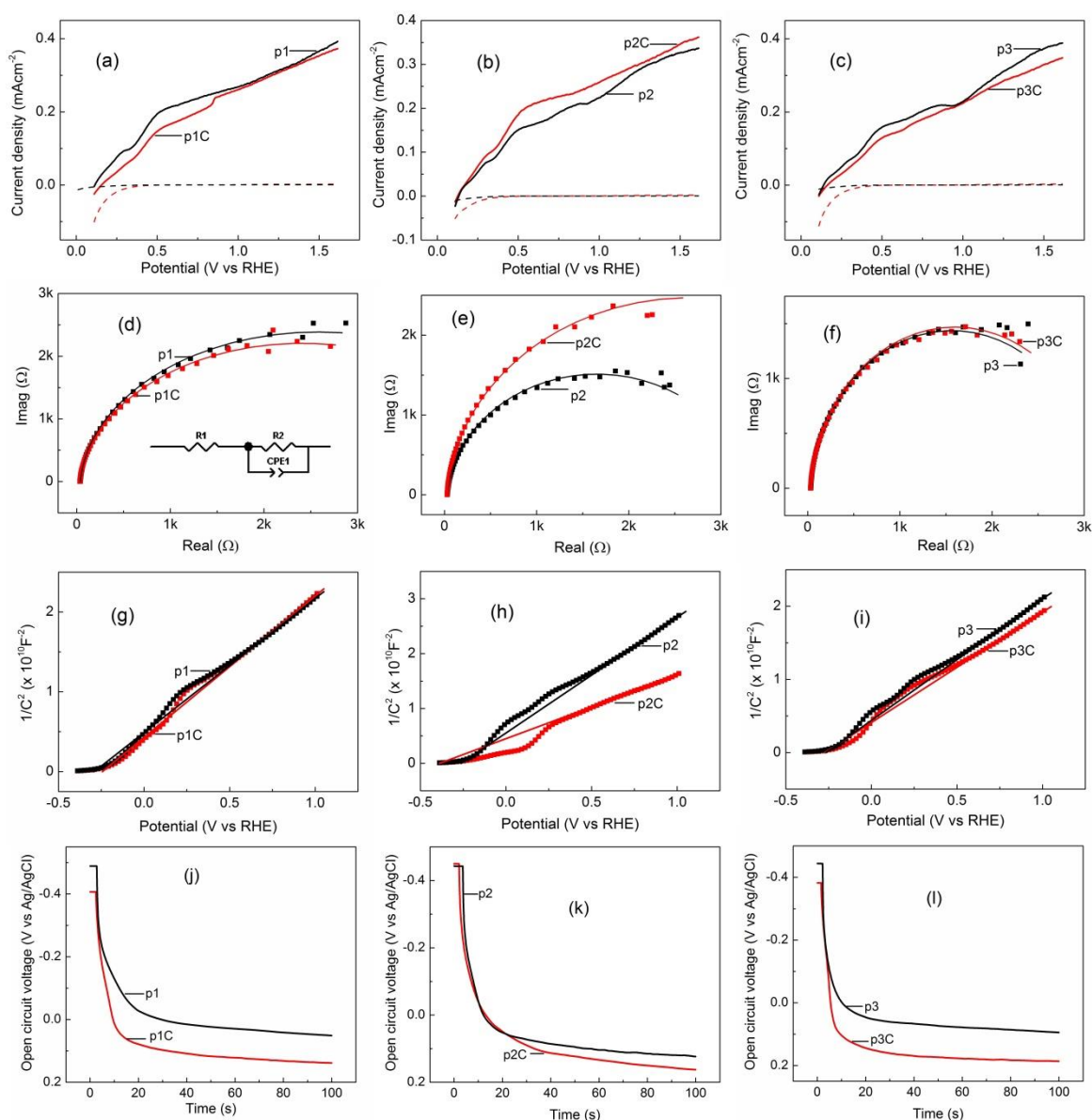


Fig. 2. J-V characteristics curves obtained under simulated solar illumination (a, b, c) and dark, EIS Nyquist plots (inset: equivalent circuit for simulation photoelectrochemical mechanism in photoelectrodes) (d, e, f), Mott-Schottky plots (g, h, i) and open circuit voltage decay with time, after stopping the illumination (j, k, l) for samples p1, p1C, p2, p2C, p3, p3C in solution of 0.5 M Na₂SO₄, pH=7.

In this model, R1 is associated with the resistance of the material itself and R2 is the resistance of the charge transfer between the electrolyte and the electrode, CPE1 element is correlated with space-charge-layer capacitance. Table 2 shows the values of these parameters for all measured samples. It shows a decrease in resistance R1 of samples p2 and p3 after their treatment with nanocarbon. Mott-Schottky analysis shows higher values for charge carrier density N_d (Table 3) of samples p2C and p3C which is consistent with changes in resistance R1 of samples p2 and p3 observed in Table 2. Both N_d and the flat-band potential (E_{fb}) for the semiconductor/electrolyte interface were determined using Mott-Schottky equation:

$$\frac{A_s}{C_{sc}^2} = \left(\frac{2}{e_0 \epsilon \epsilon_0 N_d} \right) \left((E - E_{fb}) - \frac{kT}{e_0} \right) \quad (1)$$

where A_s is surface area of the electrode, C_{sc} is the specific capacitance of space-charge layer ($F\text{ cm}^{-2}$), e_0 is the equivalent electron charge ($1.602 \times 10^{-19}\text{ C}$), ϵ is the dielectric constant of TiO_2 (48) [20] ϵ_0 is the permittivity of vacuum ($8.854 \times 10^{-14}\text{ F cm}^{-1}$), N_d is the carrier density, E is the applied potential, E_{fb} is the flat-band potential, k is Boltzmann constant ($1.38 \times 10^{-23}\text{ J K}^{-1}$) and T is absolute temperature. N_d resulted from Mott-Schottky plots is of 10^{20} order and values for flat-band potential of the samples are slightly different; a higher value for E_{fb} was obtained for sample p2C. The positive slopes in the plot C^{-2} - E (Fig.2 g, h, i) suggest that all samples are n-type semiconductors.

Table 2. The parameters of the photoanodes obtained from impedance spectroscopy analysis.

Photoanode	R1 (Ωcm^2)	R2 (Ωcm^2)	CPE1 (Fcm^{-2})
p1	36.9	5095	1.3×10^{-5}
p1C	33	4749	1.3×10^{-5}
p2	31.2	3248	1.2×10^{-5}
p2C	28.4	5089	1.4×10^{-5}
p3	34.3	3131	1.3×10^{-5}
p3C	30.9	3069	1.4×10^{-5}
p4	37	4230	1.2×10^{-5}
p5	35.2	11826	1.1×10^{-5}

The values of the resistance R2 are high for all samples. The presence of carbon on the TiO_2 surface did not improve the charge transfer process at electrode/electrolyte interface; in the case of p2C, value of this resistance has increased, indicating even a disturbance of this process. At the same time, samples containing more carbon have higher CPE1 capacitances, suggesting a higher concentration of charges in space-charge-layer of the semiconductor.

The charge recombination process in the studied photoanodes has been evaluated by measuring the open-circuit voltage decay after interruption of the illumination (Fig.2 j, k, l). A lower decay rate is correlated with a longer lifetime of photogenerated electrons [21, 22]. As can be seen in Fig.2, the samples carbon/ TiO_2 display higher decay rate of photogenerated voltage compared with correspondent samples containing only TiO_2 film.

Table 3. Flat-band potential values and bulk donor densities (N_d) of the measured samples.

Sample	Flat-band potential (V vs RHE)	Carrier density, $N_d/10^{20}(\text{cm}^{-3})$
p1	-0.29	1.75
p1C	-0.24	1.66
p2	-0.26	1.39
p2C	-0.38	2.54
p3	-0.27	1.77
p3C	-0.27	1.95
p4	-0.37	1.62
p5	-0.28	1.80

The photoanodes based on carbon/TiO₂ composites (samples p4 and p5) were studied separately (Fig. 3). It was found that the photoelectrochemical performance decreased (Fig. 3 a) with the increase of the carbon concentration of samples (from 1wt% in p4 to 2wt% in p5).

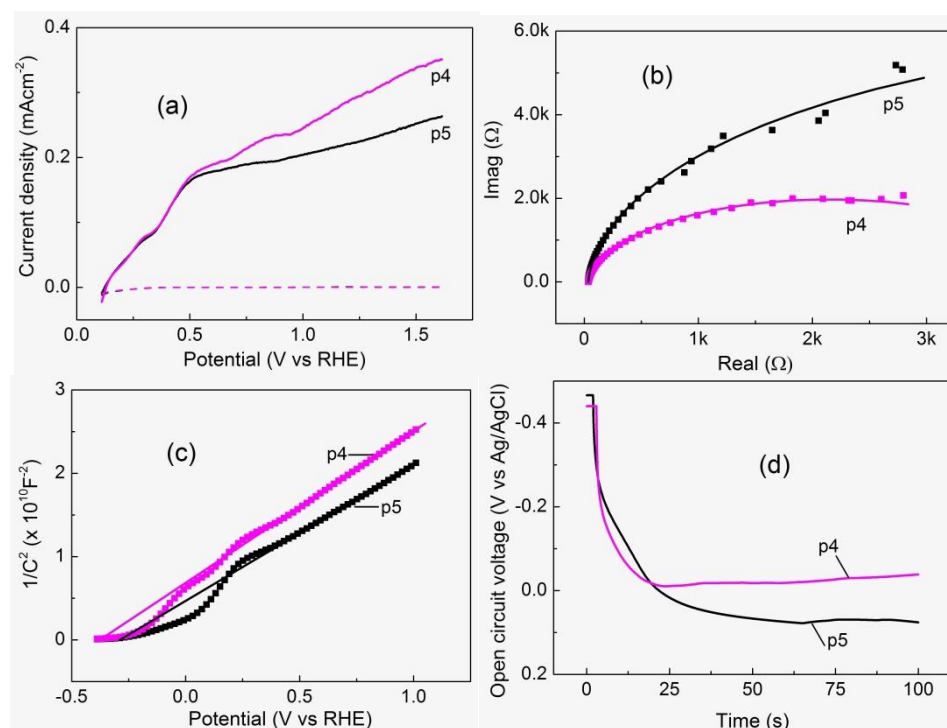


Fig. 3. J-V characteristics curves obtained under simulated solar illumination (a), EIS Nyquist plots (b), Mott-Schottky plots (c) and open circuit voltage decay with time, after stopping the illumination (d) for samples p4 and p5 in solution of 0.5 M Na₂SO₄, pH=7.

The measurements of impedance spectroscopy showed for sample p5 a decrease in the resistance R1 (Table 2, Fig. 3 b)), correlated with the increase of the value of Nd (Table 3, Fig. 3c) but also a steep increase of R2. Also, the increase in carbon content led to a decrease in the lifetime of photogenerated electrons (Fig. 3d, sample p5).

4. Conclusions

In summary, nanocarbon decorated TiO₂ photoanodes were successfully prepared via spray coating method. Comparatively, nanocarbon/TiO₂ composites with low carbon content were studied. The presence of carbon on the TiO₂ surface did not improve the charge transfer process at electrode/electrolyte interface. The samples carbon/TiO₂ display lower lifetimes of photogenerated electrons compared with correspondent samples containing only TiO₂ film. The small enhancement of photoelectrochemical performance of these photoanodes was attributed to increased charge carrier density.

Acknowledgements

The financial support of Romanian Ministry of Education and Research (Core Program PN19-03, contract no. 21 N/08.02.2019) is gratefully acknowledged.

References

- [1] A. J. Cowan, J. Tang, W. Leng, J. R. Durrant, D. R. Klug, *J. Phys. Chem. C* **114** (9), 4208 (2010).
- [2] R. Dholam, N. Patel, M. Adami, A. Miotello, *Int. J. Hydrogen Energy* **34** (13), 5337 (2009).
- [3] J. Tang, J. R. Durrant, D. R. Klug, *J. Am. Chem. Soc.* **130** (42), 13885 (2008).
- [4] R. Abe, *J. Photochem Photobiol C* **11** (4), 179 (2010).
- [5] S. Kment, F. Riboni, S. Pausova, L. Wang, L. Wang, H. Han, Z. Hubicka, J. Krysa, P. Schmuki, R. Zboril, *Chem. Soc. Rev.* **46** (12), 3716 (2017).
- [6] M. D. Stamate, *Thin Solid Films* **372** (1-2), 246 (2000).
- [7] L. Forro, O. Chauvet, D. Emin, L. Zuppiroli, H. Berger, F. Levy, *J. Appl. Phys.* **75** (1), 633 (1994).
- [8] N. Fajrina, M. Tahir, *Int J Hydrogen Energy* **44** (2), 540 (2019).
- [9] D. Sudha, P. Sivakumar, *Chem Eng Process* **344** (97), 112 (2015).
- [10] M-Y Xie, K-Y Su, R-J Wu, M. Chavali, W-C Chang, *J.Taiwan Inst Chem E* **70**, 161 (2017).
- [11] R. A. Rather, S. Singh, B. Pal, *Sol. Energy Mater Sol Cells* **160**, 463 (2017).
- [12] X. Yan, , Z. Jia, H. Che, S. Chen, P. Hu, J. Wang, L. Wang, *Appl Catal B* **234**, 19 (2018).
- [13] Q. Wei, X. Yan, Z. Kang, Z. Zhang, S. Cao, Y. Liu, Y. Zhang, *J. Electrochem. Soc.* **164** (7), H515 (2017).
- [14] S. Xie, H.Su, W. Wei, M. Li, Y. Tong, Z. Mao, *J. Mater. Chem. A* **2** (39), 16365 (2014).
- [15] Y. Su, P. Chen, F. Wang, Q. Zhang, T. Chen, Y. Wang, K. Yao, W. Lv, G. Liu, *RSC Adv.* **7**, 34096 (2017).
- [16] P.Ren, X.Fu, Y. Zhang, *Catal Lett* **147**, 1679 (2017).
- [17] L. M. Pastrana-Martínez, S. Morales-Torres, S. K. Papageorgiou, F. K. Katsaros, G. E. Romanos, J. L. Figueiredo, J. L. Faria, P. Falaras, A. M.T. Silva, *Appl Catal B: Environ* **142-143**, 101 (2013).
- [18] M. Sima, E. Vasile, A. Sima, *Thin Solid Films* **658**, 7 (2018).
- [19] S. Zhang, L. Zhang, L. Huang, G. Zheng, P. Zhang, Y. Jin, Z. Jiao, X. Sun, *J. Lumin.* **206**, 608 (2019).
- [20] L. Xiao, T. Liu, M. Zhang, Q. Li, J. Yang, *ACS Sustainable Chem. Eng.*, **7** (2), 2483 (2019).
- [21] B.H. Meekins, P.V. Kamat, *ACS Nano* **3** (11), 3437 (2009).
- [22] J. Bisquert, A. Zaban, M. Greenshtein, I. Mora-Sero, *J. Am. Chem.Soc.* **126** (41), 13550 (2004).